Synsint Research Group

Available online at www.synsint.com

Synthesis and Sintering

ISSN 2564-0186 (Print), **ISSN** 2564-0194 (Online)

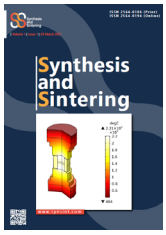

Research article

Pulsed electric current sintering of TiB_2-based ceramics using nitride additives

Naeimeh Sadat Peighambardoust [a,*], Çağın Çevik [b], Tannaz Assar [c], Sunghoon Jung [d], Seon Yong Lee [e], Joo Hwan Cha [f,*]

[a] *Koç University Boron and Advanced Materials Applications and Research Center (KUBAM), Sariyer, Istanbul, 34450, Turkey*
[b] *Department of Biophysics, Istanbul University-Cerrahpasa, Istanbul, Turkey*
[c] *Department of Geophysical Engineering, Istanbul Technical University, Istanbul, Turkey*
[d] *Advanced Nano Surface Department, Korea Institute of Materials Science, Changwon, 51508, Republic of Korea*
[e] *Department of Materials Science and Engineering, Research Institute of Advanced Materials, Seoul National University, Seoul 08826, Republic of Korea*
[f] *Innovative Enterprise Cooperation Center, Korea Institute of Science & Technology, Hwarangro 14-gil, Seongbuk-gu, Seoul 02792, Republic of Korea*

A B S T R A C T

In this research, various types of nitride additives were incorporated into titanium diboride attaining dense TiB_2-based ceramics by field-assisted sintering technique. The addition of different types of nitride additives, namely Si_3N_4, BN, AlN, and TiN, significantly improved the sinterability of TiB_2, achieving near fully dense ceramics. The X-ray diffraction analysis and microstructural evaluation confirmed the presence of the h-BN compound in all specimens. In the TiB_2-Si_3N_4 ceramic, Si_3N_4 additive reacted with B_2O_3 oxide, in-situ generating h-BN, and SiO_2 phases. Although the h-BN phase was produced in the TiB_2-AlN specimen, the main proportion of AlN remained in the sample as an unreacted ex-situ phase. In terms of the TiB_2-TiN ceramic, some of the nitrogen and boron atoms could leave the TiN and TiB_2 crystalline structures, contributing to the in-situ formation of h-BN.

K E Y W O R D S

Titanium diboride
Silicon nitride
Hexagonal boron nitride
Aluminum nitride
Titanium nitride
Field assisted sintering technique

OPEN ACCESS

1. Introduction

As an ultra-high-temperature ceramic (UHTC), TiB_2 possesses many magnificent advantages, such as high melting point, great hardness, good wear resistance, good thermal conductivity, high Young's modulus, and relatively low coefficient of thermal expansion [1–5]. Having such diverse features has made TiB_2 an appropriate candidate for several applications, including armors, cutting tools, turbine blades, Hall-Heroult cells' cathodes, abrasion, and corrosion resistance compounds, etc. [6, 7]. However, this notable substance had some demerits, e.g. low self-diffusion coefficient, surface oxide layers (TiO_2, B_2O_3), and strong covalent bonding, which make its sinterability problematic [8–10].

According to the previous studies, reaching a near fully dense TiB_2 material needs both a high sintering temperature and a very high external pressure (~3 GPa). However, implementing a high sintering temperature results in grain coarsening, which deteriorates both fracture toughness and flexural strength [11–13]. Accordingly, quite a few researches have been carried out to elevate the sinterability of TiB_2 substances by incorporating different additives [14–22]. Although the addition of a metallic additive boosts the sinterability of TiB_2, the high-temperature qualities of the resulted material may be adversely affected thanks to the low melting temperature of the metallic ingredient [23, 24]. However, a suitable ceramic secondary phase not only can improve the sintering behavior but also can have positive impacts on the mechanical features [25–27]. On the other hand, utilizing an

* Corresponding authors. *E-mail addresses:* npeighambardoust@ku.edu.tr (N.S. Peighambardoust), jhcha@kist.re.kr (J.H. Cha)
Received 15 March 2021; Received in revised form 5 April 2021; Accepted 5 April 2021.

https://doi.org/10.53063/synsint.2021.1112

advanced sintering technique like spark plasma sintering (SPS) can significantly remove obstacles against the production of high-quality ceramics owing to the unique merits of such a process, namely short dwelling time, high applied external pressure, and relatively low sintering temperature [28–32].

Several papers have been published on the TiB_2-based composites incorporated by various nitrides as sintering aids/reinforcements. Júnior et al. [20] studied the impact of sintering temperature on the sinterability of TiB_2-30 vol% AlN. According to their results, the best relative density value of almost 95% was attained for the sample sintered at 1900 °C, which was around 20% higher than that at 1500 °C. Moreover, some in-situ compounds, i.e., h-BN, Al_2O_3, TiN, and AlB_2, were produced over the sintering process. The incorporation of low content of AlN additive (5 wt%) in the TiB_2 system was also investigated by Nguyen et al. [30]. The composite sample reached its near fully dense density, manifesting the beneficial role of AlN as a sintering aid. Besides, both microstructural observations and XRD patterns verified the in-situ formation of the h-BN ingredient owing to a chemical reaction between the introduced AlN and the surface oxide of B_2O_3. The TiB_2-BN system was also studied by Nguyen et al. [7]. It was reported that the nucleation and growth of nano-sized BN platelets had a significant effect on the sinterability of such a system, reaching a near fully dense composite. The same phenomenon occurred when 5 wt% TiN was added to TiB_2 as an additive, leading to a sample with a relative density of more than 99% [33]. The influence of various weight percentages of Si_3N_4 on the relative density of TiB_2-based ceramics was assessed by Park et al. [34]. The hot-pressing technique at 1800 °C was used to fabricate specimens in this research. A low content of Si_3N_4 (2.5 wt%) significantly improved the sinterability of TiB_2 thanks to the elimination of TiO_2 surface oxide as well as the in-situ formation of h-BN, TiN, and SiO_2 compounds. However, the addition of more Si_3N_4 resulted in a reduction in the relative density of samples. Finally, Mahaseni et al. [35] also produced a fully dense TiB_2-5 wt% Si_3N_4 composite using the SPS route at 1900 °C. The in-situ formation of the h-BN, TiN, and SiO_2 phases were verified in this study, too.

Although the impact of various nitride additives on the properties of TiB_2 was scrutinized in different studies, this investigation has tried to assess the microstructural development and sinterability of various TiB_2-nitride (Si_3N_4, h-BN, AlN, and TiN) composites in a single research work. The SPS process was implemented to fabricate the targeted specimens, and subsequently, the SPSed samples were characterized using XRD and FESEM.

2. Experimental procedure

Table 1 presents the initial materials used in this investigation and their relevant characteristics. Table 2 also exhibits the composition of five different specimens designed to compare the role of various nitrides on the characteristics of TiB_2-based ceramics. Initially, a digital scale was implemented to weigh the required ingredients for any sample. Next, the powder mixtures were scattered using an ultrasonic facility for 0.5 h in ethanol. After that, a hot-plate agitator was used (3 h, 120 °C) for both extra mixing and removing the ethanol medium. Subsequently, the prepared slurries were put into a Universal oven for complete dehumidification at 110 °C for 24 h. Next, in order to reach homogeneous powder mixtures, as well as refining the powder particles, each powder sample was separately wet- mixed using a ball-mill device. Regarding ball-milling parameters, each mixture, together with 50 cc ethanol, was poured into a zirconia cup. The ratio of balls/powder was 10:1, and the ball-milling was carried out at 200 rpm for 5 h. Next, powder mixtures were dehumidified for 24 h at 100 ºC using an oven. After that, the dried slurries were smashed and passed through a 100-mesh sieve. A graphite die was used for loading the powder mixtures in it, which was lined by a graphite foil, too. Ultimately, a spark plasma sintering machine was utilized to sinter the specimens at 1850 °C for 8 min under 35 MPa. The final ceramics were disk-shaped with 30 mm diameter and 7 mm in height.

Table 1. List of the raw powders and their relevant information.

Powder	Particle size (µm)	Purity (%)
TiN	< 5	> 98.5
AlN	< 4	> 98.4
h-BN	< 2	> 98.0
Si_3N_4	< 3	> 98.1
TiB_2	< 8	> 98.7

The fraction of bulk to the theoretical density of each ceramic was recorded as the relative density. The bulk density was estimated using the Archimedes principle, while the theoretical one was calculated using the rule of mixture. An X-ray diffractometer (XRD) was used for phase analysis, whereas the elemental evaluation was carried out using energy-dispersive X-ray spectroscopy (EDS). The latter device was coupled with a field emission scanning electron microscopy (FESEM), which was utilized for microstructural investigation on polished and fracture surfaces. Moreover, an X-ray fluorescence device (XRF) was employed to analyze the exact composition of the initial TiB_2 powder. Finally, the thermodynamic study was fulfilled using another computer program named HSC chemical package.

3. Results and discussion

3.1. Thermodynamic assessment and sinterability

Based on the SEM images and XRD patterns (not presented here) of the raw substances used in this investigation, the morphology and particle size of the powders were in agreement with those claimed by the manufacturer in Table 1. In addition, identifying no peak except the base materials in all XRD patterns indicates the high-purity of the as-purchased powders (see Table 3 for XRF analysis of the TiB_2 powder). However, it is a recognized fact that all these raw materials are covered by some oxide phases, namely TiO_2 and B_2O_3 (for TiB_2), SiO_2 (for Si_3N_4), B_2O_3 (for BN), Al_2O_3 (for AlN), and TiO_2 (for TiN). The presence of such oxides, especially on the matrix powder, may lead to

Table 2. Composition of the as-sintered samples.

Sample	Matrix	Sintering aid
Monolithic TiB_2	TiB_2	-
TiB_2-Si_3N_4	TiB_2	4 wt% Si_3N_4
TiB_2-BN	TiB_2	4 wt% BN
TiB_2-AlN	TiB_2	4 wt% AlN
TiB_2-TiN	TiB_2	4 wt% TiN

partial densification. In short, surface oxides negatively affect consolidation behavior in two different ways. On the one hand, they hinder proper bonding among the particles during the sintering process, and on the other hand, they promote grain coarsening. Subsequently, the most important role of an additive in these kinds of sintering systems could be the annihilation of the surface oxides [36–38]. The influence of various nitride additives on this phenomenon will be discussed in the following section.

Fig. 1 compares the beneficial impact of each nitride additive on the relative density of the SPSed ceramics. As can be seen in this bar chart, the monolithic TiB_2 hit a relative density of 94.9%, which implies more than 5% remaining porosity in the undoped ceramic. Nevertheless, the incorporation of all nitride additives, namely Si_3N_4, h-BN, AlN, and TiN, promotes the sintering behavior of TiB_2, resulting in four near fully dense composites. Although the relative density values of the composite specimens were roughly similar, the routes through which these additives could improve the sinterability of TiB_2 may be different. Accordingly, the influence of each nitride on the sintering behavior of TiB_2 was individually studied and linked to the relevant XRD outcome.

Firstly, understanding the sintering mechanism of the monolithic TiB_2 looks advantageous. The XRD pattern of the TiB_2 sample (Fig. 2) indicates that just TiB_2 peaks were detectable. As noted earlier, initial TiB_2 particles contain surface oxides, namely TiO_2 and B_2O_3. These oxide compounds have some harmful impacts on the sintering behavior of TiB_2, namely hindering strong bonding between the TiB_2 particles, and grain coarsening.

According to the XRD pattern of the TiB_2-Si_3N_4 ceramic, it seems as if the whole content of the additive was consumed over the SPS process, participating in producing the in-situ h-BN phase. Eq. 1 presents the possible chemical reaction through which the in-situ h-BN may be generated. The feasibility of such a reaction was evaluated through the estimation of its ΔG° at 1850 °C (-281 kJ), and as a result, Eq. 1 can be advanced in the present sintering system. Excluding the produced h-BN compound, an oxide phase, namely SiO_2, may also form based on this equilibrium. The presence of the SiO_2 peaks in the XRD pattern of the TiB_2-Si_3N_4 sample fortifies the possibility of progressing Eq. 1 over the SPS. By contrast, the in-situ created the SiO_2 phase and that, from the surface oxide on the Si_3N_4 particles can create a low melting point compound with B_2O_3 [39]. This molten phase can be beneficial in promoting the chemical reaction in Eq. 1 through assisting mass transfer. The remaining liquid phase would fill the unclosed cavities, increasing the relative density of the sample.

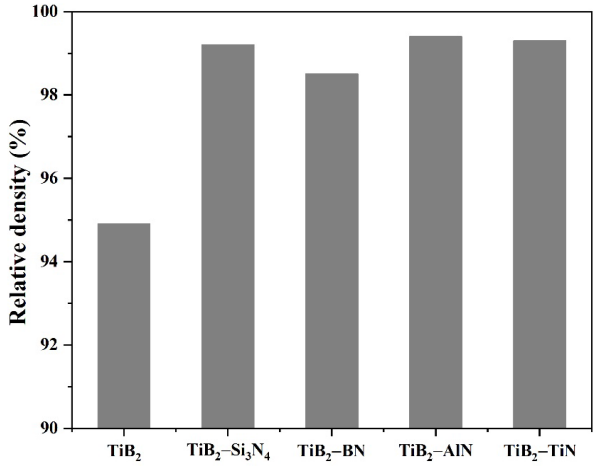

Fig. 1. The relative density of the as-sintered samples.

Table 3. XRF analysis of the initial TiB_2 powder.

Elements	Ti	B	C	N	H	O
wt%	68.1	30.0	0.35	0.27	0.41	0.87

$$Si_3N_4 + 2B_2O_3(l) = 3SiO_2 + 4BN \quad (1)$$

The XRD pattern of the TiB_2-AlN specimen clearly shows that both AlN and BN phases were available in the sample, along with the TiB_2 matrix. Eq. 2 proposes the possible chemical interaction through which the in-situ BN can be produced. This equation is favorable at the current sintering conditions thanks to its highly negative ΔG° at 1850 ° C (-177 kJ). According to Eq. 2, the Al_2O_3 oxide was also the other product of the reaction, increasing the Al_2O_3 content of the system, which was available as the surface oxide on the initial AlN particles. It is also worth mentioning that the Al_2O_3 content can react with B_2O_3, forming several compounds like $Al_{18}B_4O_{33}$ and $Al_4B_2O_9$ [40]. The reason for not detecting Al_2O_3 in the relevant XRD result could be due to the advancement of such reactions. As a result, the content of each Al-based compound has been below the limit that the XRD device was able to detect.

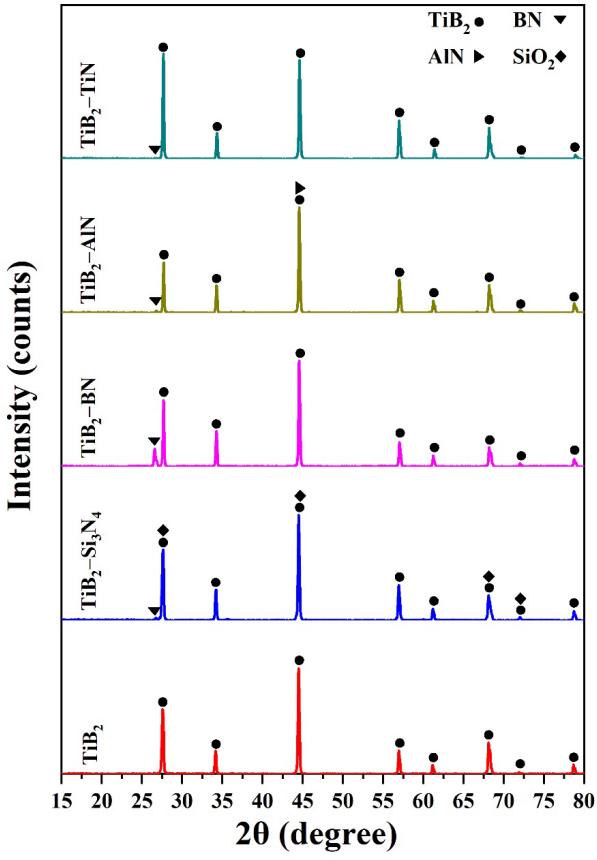

Fig. 2. XRD patterns of the as-sintered samples.

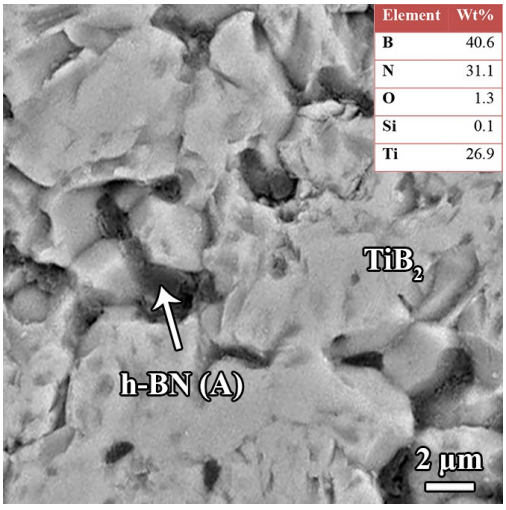

Fig. 3. FESEM micrograph of the polished surface of the TiB_2-Si_3N_4 sample.

$$2AlN + B_2O_3(l) = 2BN + Al_2O_3 \quad (2)$$

Fig. 2 also illustrates the XRD pattern of the TiB_2-TiN sample. Although identifying no peak related to the TiN phase implies its full consumption over the SPS process, the thermodynamic assessment revealed that such a thing could not be possible. However, a partial interaction between the introduced TiN and the TiB_2 matrix could happen, leading to the in-situ formation of h-BN. According to the literature [41], when TiB_2 and TiN coexist under the SPS circumstances at high temperatures, TiN can lose nitrogen, and TiB_2 can lose boron. In this way, the free nitrogen and boron can form a BN ingredient, which is in harmony with the corresponding XRD result. On the other hand, Kitiwan et al. [42] reported that in a TiB_2-TiN system, the exited boron atom from the TiB_2 crystalline structure could dissolve into the TiN phase, forming a solid solution. In other words, TiN not only can lose N but also can absorb B atoms. This phenomenon can roughly justify why no peak associated with TiN was

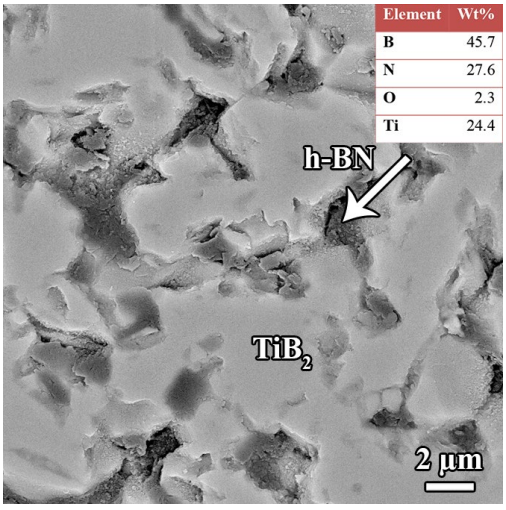

Fig. 4. FESEM micrograph of the polished surface of the TiB_2-BN sample.

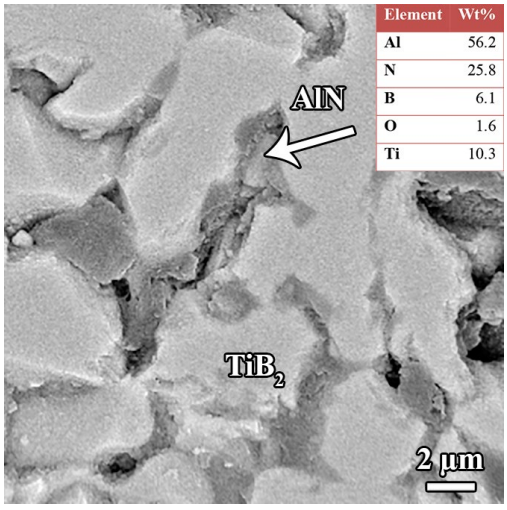

Fig. 5. FESEM micrograph of the polished surface of the TiB_2-AlN sample.

identified in the attributing pattern. Comparing the XRD pattern of the TiB_2-TiN sample with the other TiB_2-based ceramics in this investigation shows that some TiB_2 peaks were shifted to the higher degrees (around 0.5 °), fortifying the above-mentioned assumption. However, it sounds that the formation of the in-situ h-BN compound has had a significant influence on improving the relative density of this composite. Indeed, other factors such as grain refining, adding a finer secondary phase, etc. were also effective in promoting the sintering behavior of these TiB_2-based materials.

3.2. Microstructural study

Figs. 3–6 compare the corresponding micrographs from the polished surfaces of the SPSed samples. As can be seen, all micrographs comprise a bright-colored TiB_2 matrix in which a grey-colored secondary phase is distributed. The relevant EDS point analysis was fulfilled from these phases, and the results were attached to the attributing FESEM images. According to these EDS outcomes, the dominant secondary phase was BN in the samples incorporated with Si_3N_4, BN, and TiN, while the dark phase in the TiB_2-AlN specimen was associated with the remaining AlN. As shown clearly, the source of the BN phase was different in the TiB_2-BN composite, compared to TiB_2-Si_3N_4 and TiB_2-TiN. Briefly, the TiB_2-BN sample contained the ex-situ BN, while such a phase was formed as an in-situ compound in the others. In addition, no apparent pore can be seen in the micrographs of the composite samples, confirming the relative density results. However, the cavities related to the pulled-out secondary phase(s) over the polishing may be mistaken for the pores that should be taken into account.

The FESEM fractograph of the TiB_2-Si_3N_4 is also illustrated in Fig. 7. Looking at this image, some solidified glassy phase can be seen. According to the explanation in the "thermodynamic assessment and sinterability" section, this glassy phase mainly consists of the TiO_2 oxide in the monolithic sample. The other oxide compound, namely B_2O_3, was possibly evaporated and left the system owing to the high applied vacuum. However, as explained earlier, more liquid phase can be formed in the sample containing Si_3N_4, compared to the monolithic TiB_2 (shiny surfaces and round edges in Fig. 7 proves the formation of liquid phase in this composite over sintering). This observation is in

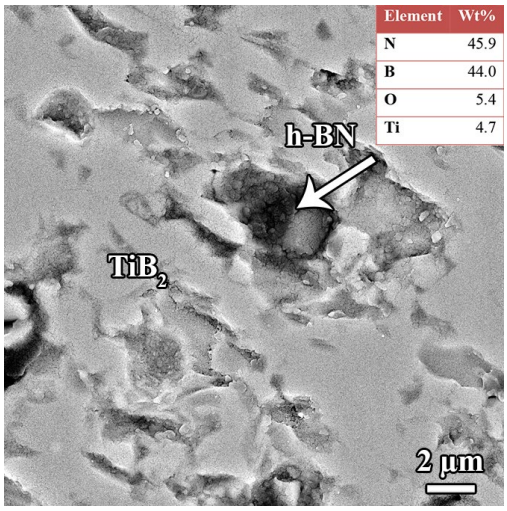

Fig. 6. FESEM micrograph of the polished surface of the TiB_2-TiN sample.

agreement with the contribution of the SiO_2 oxide in creating a limited content of the liquid phase. The formation of h-BN platelets in this fractograph is utterly apparent.

4. Conclusions

The incorporation of several nitrides, namely Si_3N_4, BN, AlN, and TiN, into the microstructural features and sinterability of TiB_2-based composites was studied. All these additives had a remarked influence on the relative density of TiB_2, obtaining four near fully dense samples. The XRD results, along with the microstructural evaluation, confirmed the presence of the h-BN phase in the microstructure of all SPSed specimens. However, the main proportion of the AlN additive remained in the TiB_2-AlN sample as an unreacted phase. In terms of the TiN additive, some of the N atoms left the crystalline structure of TiN, forming the BN compound through interacting with the exited B from TiB_2.

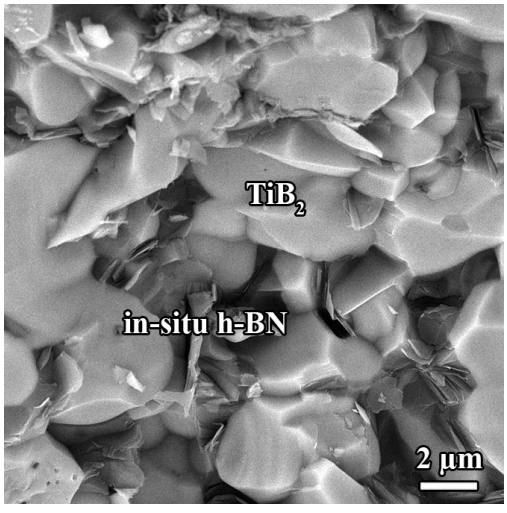

Fig. 7. FESEM fractograph of the TiB_2-Si_3N_4 sample.

CRediT authorship contribution statement

Naeimeh Sadat Peighambardoust: Conceptualization, Writing – original draft, Supervision.
Çağın Çevik: Writing – review & editing.
Tannaz Assar: Software.
Sunghoon Jung: Data curation, Methodology.
Seon Yong Lee: Investigation, Resources.
Joo Hwan Cha: Validation, Writing – review & editing.

Data availability

The data underlying this article will be shared on reasonable request to the corresponding author.

Declaration of competing interest

The authors declare no competing interests.

Funding and acknowledgment

The authors express their deepest gratitude to their affiliated universities and esteemed research institutes in Turkey and Republic of Korea for their support, which have been instrumental in facilitating this international inter-university research collaboration. They extend their appreciation to the academic and research communities of both countries for fostering an environment of collaboration and knowledge exchange.

References

[1] M.M. Mokhayer, M.G. Kakroudi, S.S. Milani, H. Ghiasi, N.P. Vafa, Investigation of AlN addition on the microstructure and mechanical properties of TiB2 ceramics, Ceram. Int. 45 (2019) 16577–16583. https://doi.org/10.1016/j.ceramint.2019.05.196.
[2] F. Ghafuri, M. Ahmadian, R. Emadi, M. Zakeri, Effects of SPS parameters on the densification and mechanical properties of TiB2-SiC composite, Ceram. Int. 45 (2019) 10550–10557. https://doi.org/10.1016/j.ceramint.2019.02.119.
[3] D. Demirskyi, H. Borodianska, Y. Sakka, O. Vasylkiv, Ultra-high elevated temperature strength of TiB2-based ceramics consolidated by spark plasma sintering, J. Eur. Ceram. Soc. 37 (2017) 393–397. https://doi.org/10.1016/j.jeurceramsoc.2016.08.009.
[4] F. Rezaei, M.G. Kakroudi, V. Shahedifar, N.P. Vafa, M. Golrokhsari, Densification, microstructure and mechanical properties of hot pressed tantalum carbide, Ceram. Int. 43 (2017) 3489–3494. https://doi.org/10.1016/j.ceramint.2016.10.067.
[5] N. Wu, F. Xue, H. Yang, G. Li, F. Luo, J. Ruan, Effects of TiB2 particle size on the microstructure and mechanical properties of TiB2-based composites, Ceram. Int. 45 (2019) 1370–1378. https://doi.org/10.1016/j.ceramint.2018.08.270.
[6] L.A.F. Peçanha, S.N. Monteiro, Í. do V. Tomaz, M.M. de Oliveira, A.M. Ramalho, et al., Characterization of TiB2-AlN composites for application as cutting tool, J. Mater. Res. Technol. 7 (2018) 550–553. https://doi.org/10.1016/j.jmrt.2018.07.010.
[7] T.P. Nguyen, Z. Hamidzadeh Mahaseni, M. Dashti Germi, S.A. Delbari, Q. Van Le, et al., Densification behavior and microstructure development in TiB2 ceramics doped with h-BN, Ceram. Int. (2020) 18970–18975. https://doi.org/10.1016/j.ceramint.2020.04.223.
[8] S.-R. Yan, Z. Lyu, L.K. Foong, Effects of SiC amount and morphology on the properties of TiB2-based composites sintered by hot-pressing, Ceram. Int. (2020) 18813–18825. https://doi.org/10.1016/j.ceramint.2020.04.199.
[9] O. Popov, J. Vleugels, A. Huseynov, V. Vishnyakov, Reactive sintering of TiB2-SiC-CNT ceramics, Ceram. Int. 45 (2019) 22769–22774. https://doi.org/10.1016/j.ceramint.2019.07.317.

[10] F. Rezaei, M.G. Kakroudi, V. Shahedifar, N.P. Vafa, Consolidation and mechanical properties of hot pressed TaC-HfC-VC composites, Ceram. Int. 43 (2017) 15537–15543. https://doi.org/10.1016/j.ceramint.2017.08.103.
[11] K. Farhadi, A. Sabahi Namini, M. Shahedi Asl, A. Mohammadzadeh, M. Ghassemi Kakroudi, Characterization of hot pressed SiC whisker reinforced TiB2 based composites, Int. J. Refract. Met. Hard Mater. 61 (2016) 84–90. https://doi.org/10.1016/j.ijrmhm.2016.08.004.
[12] M. Shahedi Asl, A. Sabahi Namini, M. Ghassemi Kakroudi, Influence of silicon carbide addition on the microstructural development of hot pressed zirconium and titanium diborides, Ceram. Int. 42 (2016) 5375–5381. https://doi.org/10.1016/j.ceramint.2015.12.072.
[13] M. Shahedi Asl, S.A. Delbari, F. Shayesteh, Z. Ahmadi, A. Motallebzadeh, Reactive spark plasma sintering of TiB2–SiC–TiN novel composite, Int. J. Refract. Met. Hard Mater. 81 (2019) 119–126. https://doi.org/10.1016/j.ijrmhm.2019.02.022.
[14] N. Wu, F. Xue, H. Yang, H. Zhou, Y. Li, et al., Effects of WC content on core/rim phases and microstructure of TiB2-TiC-WC-(Co-Ni) cermets, Mater. Today Commun. 25 (2020) 101311. https://doi.org/10.1016/j.mtcomm.2020.101311.
[15] M. Yao, L. Chen, Z. Liu, S. Huo, S. Wang, et al., Two-step sintering of TiB2–40wt%TiN composites, Int. J. Refract. Met. Hard Mater. 84 (2019) 105037. https://doi.org/10.1016/j.ijrmhm.2019.105037.
[16] Z. Yin, J. Yuan, W. Xu, K. Liu, S. Yan, Graphene nanosheets toughened TiB2-based ceramic tool material by spark plasma sintering, Ceram. Int. 44 (2018) 8977–8982. https://doi.org/10.1016/j.ceramint.2018.02.098.
[17] Y. Wang, M. Yao, Z. Hu, H. Li, J.-H. Ouyang, et al., Microstructure and mechanical properties of TiB2-40 wt% TiC composites: Effects of adding a low-temperature hold prior to sintering at high temperatures, Ceram. Int. 44 (2018) 23297–23300. https://doi.org/10.1016/j.ceramint.2018.09.048.
[18] T. Matsuda, Synthesis and sintering of TiC-TiB2 composite powders, Mater. Today Commun. 22 (2020) 101457. https://doi.org/10.1016/j.mtcomm.2020.101457.
[19] K. Cymerman, D. Oleszak, M. Rosinski, A. Michalski, Structure and mechanical properties of TiB2/TiC–Ni composites fabricated by pulse plasma sintering method, Adv. Powder Technol. 29 (2018) 1795–1803. https://doi.org/10.1016/j.apt.2018.04.015.
[20] L.A.F. Júnior, Í.V. Tomaz, M.P. Oliveira, L. Simão, S.N. Monteiro, Development and evaluation of TiB2–AlN ceramic composites sintered by spark plasma, Ceram. Int. 42 (2016) 18718–18723. https://doi.org/10.1016/j.ceramint.2016.09.010.
[21] Y. Liu, Z. Li, Y. Peng, Y. Huang, Z. Huang, D. Zhang, Effect of sintering temperature and TiB2 content on the grain size of B4C-TiB2 composites, Mater. Today Commun. 23 (2020) 100875. https://doi.org/10.1016/j.mtcomm.2019.100875.
[22] N. Wu, F. Xue, J. Wang, H. Yang, F. Luo, J. Ruan, Effect of TiN addition on the microstructure and mechanical properties of TiB2-FeNi based cermets, Mater. Sci. Eng. A. 743 (2019) 546–557. https://doi.org/10.1016/j.msea.2018.11.067.
[23] Z. Fu, R. Koc, Sintering and mechanical properties of TiB2-TiC-Ni using submicron borides and carbides, Mater. Sci. Eng. A. 676 (2016) 278–288. https://doi.org/10.1016/j.msea.2016.08.110.
[24] J. Liu, W. Chen, L. Chen, Z. Xia, H. Xiao, Z. Fu, Microstructure and mechanical behavior of spark plasma sintered TiB2/Fe-15Cr-8Al-20Mn composites, J. Alloys Compd. 747 (2018) 886–894. https://doi.org/10.1016/j.jallcom.2018.03.113.
[25] V. Shahedifar, M. Ghassemi Kakroudi, N.P. Vafa, Characterization of TaC-based fibrous-monolithic ceramics made of fibers with different core/shell volume ratios and orientations, Mater. Sci. Eng. A. 775 (2020) 138935. https://doi.org/10.1016/j.msea.2020.138935.
[26] V. Shahedifar, M.G. Kakroudi, H.R. Baharvandi, F. Rezaei, Investigation of strength, fracture toughness, and crack propagation pattern of TaC-based fibrous monoliths as a function of microstructure architecture, Int. J. Refract. Met. Hard Mater. 78 (2019) 332–339. https://doi.org/10.1016/j.ijrmhm.2018.10.013.
[27] V. Shahedifar, M.G. Kakroudi, Fracture behavior improvement of TaC-based ceramic composites by fibrous structure, Int. J. Refract. Met. Hard Mater. 71 (2018) 15–20. https://doi.org/10.1016/j.ijrmhm.2017.10.025.
[28] Y. Pazhouhanfar, A. Sabahi Namini, S. Shaddel, Z. Ahmadi, M. Shahedi Asl, Combined role of SiC particles and SiC whiskers on the characteristics of spark plasma sintered ZrB2 ceramics, Ceram. Int. 46 (2019) 5773. https://doi.org/10.1016/j.ceramint.2019.11.027.
[29] S. Shaddel, A. Sabahi Namini, Y. Pazhouhanfar, S.A. Delbari, M. Fattahi, M. Shahedi Asl, A microstructural approach to the chemical reactions during the spark plasma sintering of novel TiC–BN ceramics, Ceram. Int. 46 (2020) 15982–15990. https://doi.org/10.1016/j.ceramint.2020.03.148.
[30] T.P. Nguyen, M.D. Germi, Z.H. Mahaseni, S.A. Delbari, Q. Van Le, et al., Enhanced densification of spark plasma sintered TiB2 ceramics with low content AlN additive, Ceram. Int. 46 (2020). 22127–22133. https://doi.org/10.1016/j.ceramint.2020.05.278.
[31] A. Mohammadzadeh, A. Sabahi Namini, M. Azadbeh, A. Motallebzadeh, On the physical and mechanical properties of spark plasma sintered pure Ti and Ti-TiB composite, Mater. Res. Express. 5 (2018) 126512. https://doi.org/10.1088/2053-1591/aae057.
[32] A. Mohammadzadeh, M. Azadbeh, H. Danninger, A.S. Namini, Ti–TiB2 composites consolidated by spark plasma sintering: Reaction mechanism, characteristics of in-situ formed phases and densification behavior, Mater. Chem. Phys. 242 (2020) 122556. https://doi.org/10.1016/j.matchemphys.2019.122556.
[33] F. Shayesteh, S.A. Delbari, Z. Ahmadi, M. Shokouhimehr, M. Shahedi Asl, Influence of TiN dopant on microstructure of TiB2 ceramic sintered by spark plasma, Ceram. Int. 45 (2019) 5306–5311. https://doi.org/10.1016/j.ceramint.2018.11.228.
[34] J.-H. Park, Y.-H. Koh, H.-E. Kim, C.S. Hwang, E.S. Kang, Densification and mechanical properties of titanium diboride with silicon nitride as a sintering aid, J. Am. Ceram. Soc. 82 (2004) 3037–3042. https://doi.org/10.1111/j.1151-2916.1999.tb02199.x.
[35] Z. Hamidzadeh Mahaseni, M. Dashti Germi, Z. Ahmadi, M. Shahedi Asl, Microstructural investigation of spark plasma sintered TiB2 ceramics with Si3N4 addition, Ceram. Int. 44 (2018) 13367–13372. https://doi.org/10.1016/j.ceramint.2018.04.171.
[36] S. Rahimi, F. SharifianJazi, A. Esmaeilkhanian, M. Moradi, A.H. Safi Samghabadi, Effect of SiO2 content on Y-TZP/Al2O3 ceramic-nanocomposite properties as potential dental applications, Ceram. Int. 46 (2020) 10910–10916. https://doi.org/10.1016/j.ceramint.2020.01.105.
[37] A. Moghanian, F. Sharifianjazi, P. Abachi, E. Sadeghi, H. Jafarikhorami, A. Sedghi, Production and properties of Cu/TiO2 nano-composites, J. Alloys Compd. 698 (2017) 518–524. https://doi.org/10.1016/j.jallcom.2016.12.180.
[38] M. Alizadeh, F. Sharifianjazi, E. Haghshenasjazi, M. Aghakhani, L. Rajabi, Production of nanosized boron oxide powder by high-energy ball milling, Synth. React. Inorganic, Met. Nano-Metal Chem. 45 (2015) 11–14. https://doi.org/10.1080/15533174.2013.797438.
[39] F. Shayesteh, S.A. Delbari, Z. Ahmadi, M. Shokouhimehr, M. Shahedi Asl, Influence of TiN dopant on microstructure of TiB2 ceramic sintered by spark plasma, Ceram. Int. 45 (2019) 5306–5311. https://doi.org/10.1016/j.ceramint.2018.11.228.
[40] S.A. Decterov, V. Swamy, I.-H. Jung, Thermodynamic modeling of the B2O3–SiO2 and B2O3–Al2O3 systems, Int. J. Mater. Res. 98 (2007) 987–994. https://doi.org/10.3139/146.101555.
[41] M. Kitiwan, A. Ito, T. Goto, Spark plasma sintering of TiN-TiB2 composites, J. Eur. Ceram. Soc. 34 (2014) 197–203. https://doi.org/10.1016/j.jeurceramsoc.2013.08.034.
[42] M. Kitiwan, A. Ito, T. Goto, B deficiency in TiB2 and B solid solution in TiN in TiN–TiB2 composites prepared by spark plasma sintering, J. Eur. Ceram. Soc. 32 (2012) 4021–4024. https://doi.org/10.1016/j.jeurceramsoc.2012.06.024.